ACADEMIC
PRESS

Depth-resolved structural imaging by third-harmonic generation microscopy

Dan Oron,[a,*] Dvir Yelin,[a] Eran Tal,[a] Sefi Raz,[b] Rachel Fachima,[b] and Yaron Silberberg[a]

[a] *Department of Physics of Complex Systems, Weizmann Institute of Science, Rehovot IL-76100, Israel*
[b] *Department of Structural Biology, Weizmann Institute of Science, Rehovot 76100, Israel*

Abstract

Third harmonic generation microscopy is shown to be a robust method for obtaining structural information on a variety of biological specimens. Its nature allows depth-resolved imaging of inhomogeneities with virtually no background from surrounding homogeneous media. With an appropriate illumination geometry, third harmonic generation microscopy is shown to be particularly suitable for imaging of biogenic crystals, enabling extraction of the crystal orientation.
© 2003 Published by Elsevier Inc.

Keywords: Third harmonic generation; Multiphoton microscopy; Polarization microscopy

1. Introduction

In recent years multiphoton processes have become an important tool in microscopy and imaging, in particular due to their inherent optical sectioning capability. The multiphoton microscope borrowed its principle of operation from confocal laser scanning microscopes with two significant differences which distinguish it from confocal ones. First, multiphoton processes are excited only at the focal spot where the photon flux density is high enough for the non-linear process to occur, eliminating the need for the confocal detector pinhole. The other distinction is that the illuminating laser is typically in the infrared rather than in the visible or ultraviolet spectral regions. Using such long excitation wavelengths allows for an improved penetration depth due to lower scattering and causes less photodamage to samples.

In contrast with conventional microscopy methods, including phase microscopy and differential interference contrast (DIC) microscopy, where the measured signal is linearly proportional to the illumination intensity, multiphoton microscopy relies on the non-linear response of the medium to the electric field. In order to generate a measurable signal from a non-linear process, a strong illumination electric field has to be achieved. The advent of ultrafast laser sources in recent years has provided us with a variety of compact sources which can easily achieve peak intensities in the order of 10^{11} W/cm^2, as required for multiphoton microscopy applications, yet with low average powers, tolerable even by live specimen.

Three-dimensional multiphoton images are obtained by scanning the sample volume point-by-point. Usually, fast scanning is performed in the transverse (x and y axes) dimensions and slow scanning in the depth (z-axis) dimension. The measured signal is digitized by a computer which synchronizes the entire process, resulting in a digital image.

The most commonly used multiphoton techniques are two-photon (Denk et al., 1990) and three-photon (Maiti et al., 1997) fluorescence. The main advantage of these techniques over standard confocal fluorescence microscopy is that it prevents out-of-focus photobleaching of the fluorescent label. Recently, however, there has been a growing interest in *coherent* multiphoton processes. In coherent processes, unlike fluorescence, there is no net energy transfer to the medium. Such processes include second- (Gannaway and Sheppard, 1978; Peleg et al., 1996) and third-harmonic (Barad

et al., 1997; Canioni et al., 2001; Muller et al., 1998; Yelin and Silberberg, 1999) generation and more recently coherent anti-Stokes Raman (CARS) microscopy (Zumbusch et al., 1999), which enable imaging of unstained samples.

The lowest-order non-linear process, second harmonic generation (SHG), can only be observed in materials which do not possess inversion symmetry. While SHG microscopy has been used for biological imaging, in particular of collagen fibrils (Campagnola et al., 2002; Cox et al., 2002; Zoumi et al., 2002), most samples, including most biogenic crystals, do not exhibit SHG. In contrast, third-order non-linear process such as third-harmonic generation (THG) or CARS occur intrinsically within any sample and are thus of a much wider applicability. The spatial resolution of these methods is roughly similar to that of standard confocal microscopy.

The interpretation of multiphoton microscopy images obtained with a coherent process is more complicated than that of multiphoton fluorescence images. Fluorescence is generally non-directional, and the total signal, being the sum of the intensities emitted from all fluorescent molecules, is proportional to their number. In contrast, in a coherent process, the emitted optical field (rather than the intensity) from all molecules is summed up, taking into account its phase. When the phases are appropriate, a condition termed phase-matching, the total signal intensity is proportional to the square of the number of scatterers (Boyd, 1992). When phase-matching is not achieved the generated signal is significantly lower. Since the condition of phase-matching is dependent on the relative geometry of the illuminating beam, the signal and the medium, signals generated by a coherent process are typically directional (A comprehensive analysis of the directionality of the signal can be found in Cheng and Xie, 2002).

The method of THG microscopy in most samples is based on a peculiarity of the phase-matching conditions: The third harmonic signal vanishes completely from most bulk samples, and is generated only when the illuminating beam is focused at a small inclusion or an interface between two materials. A signal is generated even when the two materials are index matched, since the THG process relies on the non-linear susceptibility rather than on the index of refraction. THG thus provides rich structural information on the sample otherwise unattainable by standard microscopy techniques. THG is in some sense reminiscent of phase microscopy or DIC having the ability to convert variations in material composition of transparent samples into an observable signal.

Most of the experimental work on THG microscopy has taken advantage of the ability to image inhomogeneities with a high spatial and depth resolution in order to image a variety of samples on length scales ranging from a few microns to several millimeters. These samples were mostly comprised of isotropic materials so that the tensor nature of the third-order susceptibility could be neglected. The situation is significantly different when the sample is anisotropic, and in particular when it exhibits strong birefringence such as in calcite or aragonite, two polymorphs of crystalline calcium carbonate.

Third-harmonic generation has recently been used to map the anisotropy of thin films, taking advantage of the fact that due to symmetry considerations, an isotropic sample generates no THG when illuminated with circularly polarized light, regardless of its composition (Yakovlev and Govorkov, 2001). THG has also been used for depth-resolved studies of phase-transitions and anisotropy in liquid-crystals (Shelton and Shen, 1972; Yelin et al., 1999a,b). We have extended this method to obtain depth-resolved polarization images by THG (Oron et al., 2003), utilizing the fact that for crystals exhibiting strong birefringence, strong phase-matched THG is generated even from a bulk crystal at some crystal orientations (Penzkofer et al., 1988). Moreover, the polarization of the emitted THG signal reflects the crystal orientation.

In the following we first present a simple mathematical formulation of the THG process. We then present THG images of a variety of samples. Polarization THG images of several biomineralized samples are also shown.

2. Mathematical formulation of the THG process

An approximate analytical expression can be derived for THG by a linearly polarized focused beam with a gaussian spatial profile (Barad et al., 1997; Boyd, 1992). The total third harmonic intensity in the forward direction from a sample stretching from z_1 to z_2, as illustrated in Fig. 1B, can be approximated as

$$I \propto \left| \chi^{(3)} \int_{z_1}^{z_2} \frac{e^{i\Delta k \cdot z'}}{(1 + 2iz'/b)^2} \, dz' \right|^2, \qquad (1)$$

where $\Delta k = (3\omega/c)(n_\omega - n_{3\omega})$, n is the refractive index, b the focal depth of the focusing lens, $\chi^{(3)}$ the non-linear susceptibility and ω is the input laser frequency. For a bulk medium (i.e., when the medium depth is much larger than the focal depth of the focusing lens), the limits of integration can be taken to infinity resulting in

$$I \propto \begin{cases} 0, & \Delta k \leqslant 0, \\ \frac{b\Delta k}{2} e^{-b\Delta k/2}, & \Delta k > 0. \end{cases} \qquad (2)$$

Since in most materials the index of refraction decreases with increasing wavelength ("normal dispersion"), Δk is usually negative resulting in no THG from bulk media. However, when the limits of integration of Eq. (1) are finite (as in the case of an interface between two materials), a signal is generated, which is
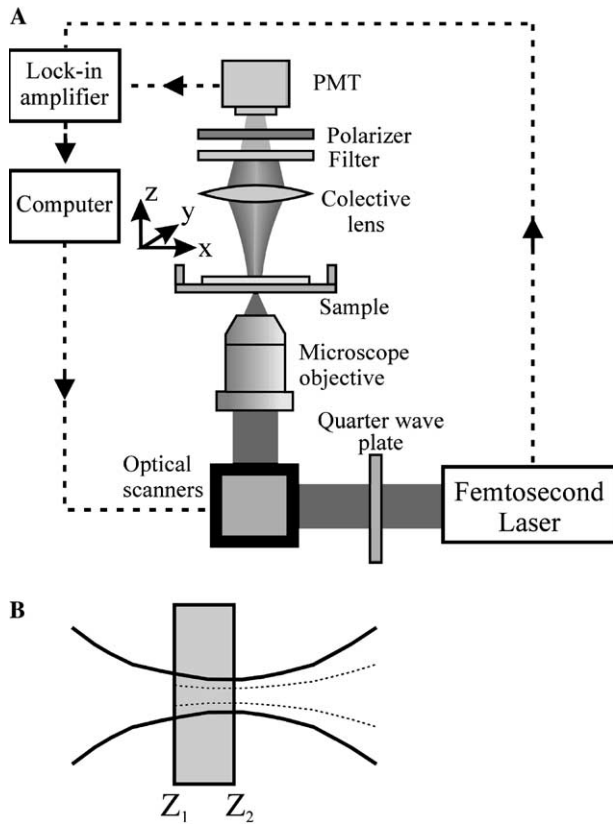
Fig. 1. (A) Outline of the THG microscope. (B) Sketch of the THG (dotted line) from a focused gaussian beam (solid line).
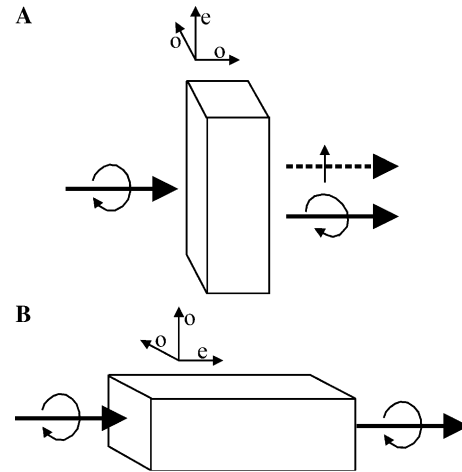

Fig. 2. Effects of strong anisotropy in a negative uniaxial crystal (such as calcite) on the fundamental (solid arrow) and the third-harmonic (dashed arrow) polarization state. (A) Beam propagation perpendicular to the extraordinary axis results in change in the polarization state of the fundamental and in phase-matched THG polarized along the extraordinary axis (B) Beam propagation parallel to the extraordinary axis. No change to the polarization state of the input beam and no THG.

proportional to the square of the difference in the non-linear susceptibilities, and is maximized when focusing at the interface between the two materials.

Two effects appear in the presence of strong birefringence in the direction of propagation of the illuminating beam, as shown schematically for a negative uniaxial crystal (such as calcite) in Fig. 2A. The first is that the polarization state of the input beam changes within the sample. The second is that in cases where the birefringence along the propagation axis of the illuminating beam is sufficiently large, it can compensate for the dispersion and change the sign of Δk in Eq. (2) from negative to positive and allow for strong THG even from a bulk crystal. This positively phase-matched signal is linearly polarized along the fast axis of the crystal (lower index of refraction) and enables to extract depth-resolved information on the crystal orientation (Oron et al., 2003). None of the two occur when the beam propagates along the extraordinary axis of such a crystal, as shown schematically in Fig. 2B.

In order to separate between the signal generated due to inhomogeneity in isotropic media, and that generated due to anisotropy the sample can be illuminated with circularly polarized light rather than with linearly polarized light. As it turns out, due to symmetry considerations, no THG is generated in isotropic media illuminated by circularly polarized light regardless of its composition. Images obtained with circularly polarized light are thus entirely due to anisotropy of the sample.

3. Materials and methods

3.1. Microscopy

As an imaging platform, we used a Zeiss Axiovert-135 microscope, which was modified into a scanning microscope. The laser source is a Spectra-Physics OPAL which provides linearly polarized 100 fs pulses with an energy of about 0.25 nJ at a wavelength of 1.5 μm at a repetition rate of 80 MHz. In experiments where circular polarization is required a zero-order quarter wave plate is inserted into the beam path. The laser beam is coupled through one of the microscope ports and is focused into the sample by a microscope objective. The focal point is scanned in the *x–y*-plane using two optical scanners, and along the *z*-axis using the motorized objective turret of the microscope. The THG signal, at 0.5 μm is collected by a condenser, passed through an analyzer, and measured by a photomultiplier tube (Hamamatsu R4220) after filtering out the excitation wavelength. The current generated by the photomultiplier is amplified using a radio-frequency lock-in amplifier (Stanford Research Systems, model SR844) which uses the synchronization output of the laser oscillator as reference. A typical integration time is 300 μs per pixel. The output signal from the lock-in amplifier is fed into a computer, which synchronizes the scanning process and the data collection.

Objectives used include a $100\times$ NA $= 1.3$ oil immersion fluar lens (Zeiss) and $10\times$ NA $= 0.25$, $20\times$ NA $= 0.45$, $60\times$ NA $= 0.85$ apochromats. All samples used were imaged through a $170\,\mu m$ cover glass and immersed in an index-matched immersion fluid. A schematic layout of the microscope is given in Fig. 1A.

3.2. Sample preparation

Three-day-old *Xenopus laevis* embryos, at the 36th developmental stage, were first fixed for 1 h in a MEMFA solution, and then transferred to methanol. Such thick biological specimen are usually opaque due to scattering, and are therefore treated with a clearing solution to render them transparent. After dehydration in methanol, the embryos were treated with a BA:BB (1 part benzyl alcohol to 2 parts benzylbenzoate) clearing solution. The preliminary treatment in methanol is required as the BA:BB clearing solution is immiscible with aqueous buffers. Albino Xenopus embryos were used in order to avoid absorption by pigments. During imaging the embryos were immersed in the clearing solution for index matching.

Seventeen-day-old fetal mouse long bones were cultured for 4–5 days in tissue culture medium supplemented with high doses antibiotics for preservation. Before imaging, the medium was gradually replaced with Methanol. Then, the Methanol was gradually replaced with a BA:BB clearing solution.

Drosophila egg-chambers were taken from wild-type females. Prior to imaging they were fixed in 4% paraformaldehyde mounted in 80% glycerol PBS. Egg-chambers were imaged on a cover glass and immersed in PBS.

Sea urchin (*Strongylocentrotus purpuratus*) skeletal larval spicules were isolated according to the procedure described in Killian and Wilt (1996). In short, spicules were isolated from fertilized embryos, centrifuged at $200g$, and repeatedly washed in 3.5% NaOCl solution, followed by washing with double-distilled water and drying. Prior to imaging, spicules were spread on a cover glass and immersed in an $n = 1.61$ index matching oil.
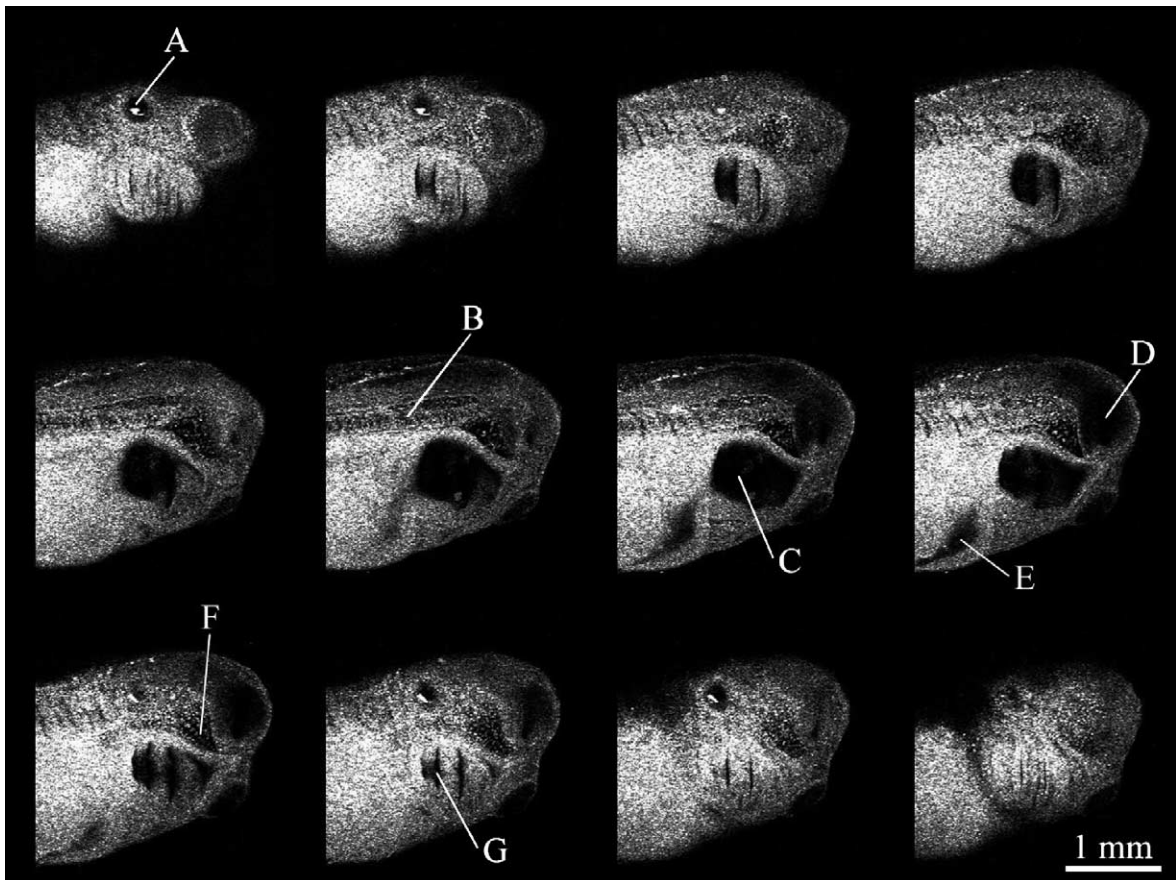

Fig. 3. Vertical sections of an albino *Xenopus laevis* embryo's head. The 3×3 mm sections are ordered according to their relative location along the *z*-axis, where the upper-left section is the closest to the objective lens and the bottom-right is the more distant part of the embryo. Sections are separated by $50\,\mu m$. The otic vesicle (A), notochord (B), foregut (C), brain ventricle (D), heart anlage (E), head mesenchyme (F), and branchial arches (G) are clearly visible.
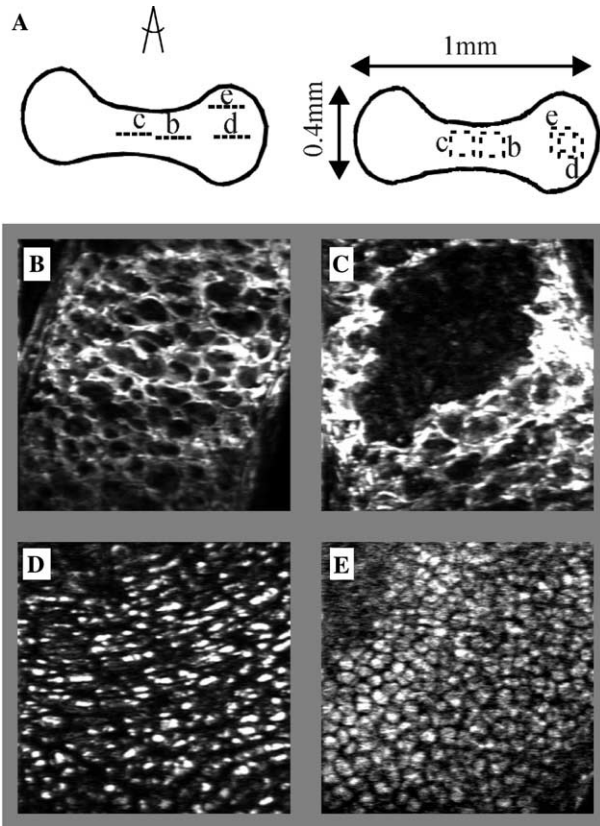
Fig. 4. THG bone sections. Four $100 \times 100\,\mu m$ sections from various locations within the bone are shown (B)–(E). In (A) a side view (left) and a top view (right) of the relative locations of these sections within the bone are shown.

Cystoliths were isolated from *Ficus microcarpa* leaves following the procedure of Arnott (1980). Freshly collected leaves were placed in a wearing blender in absolute ethanol and filtered through a cheesecloth. Cystoliths were then separated by centrifugation. Prior to imaging, cystoliths were spread on a cover glass in ethanol which was then let to dry out. After 5 min, they were immersed in an $n = 1.61$ index matching oil.

4. Results and discussion

In the following section we first present THG images of a variety of samples using linearly polarized illumination. This method highlights interfaces between materials having different non-linear susceptibilities. Since the non-linear susceptibility can vary by orders of magnitude between different materials, this method is shown to provide rich structural information on practically any sample of biological origin.

On a large scale (a few millimeters) the inhomogeneity of biological objects usually originates from the distribution of different cell types. Such a distribution of multicellular structures is reflected in the THG image. The large field of view necessary for visualization of such large structures is covered using a small magnification objective with a long working distance. Hence depth resolution is much smaller (about 50 μm for 10×, NA = 0.25 objective) compared with transversal resolution which remains good (about 2 μm). THG optical

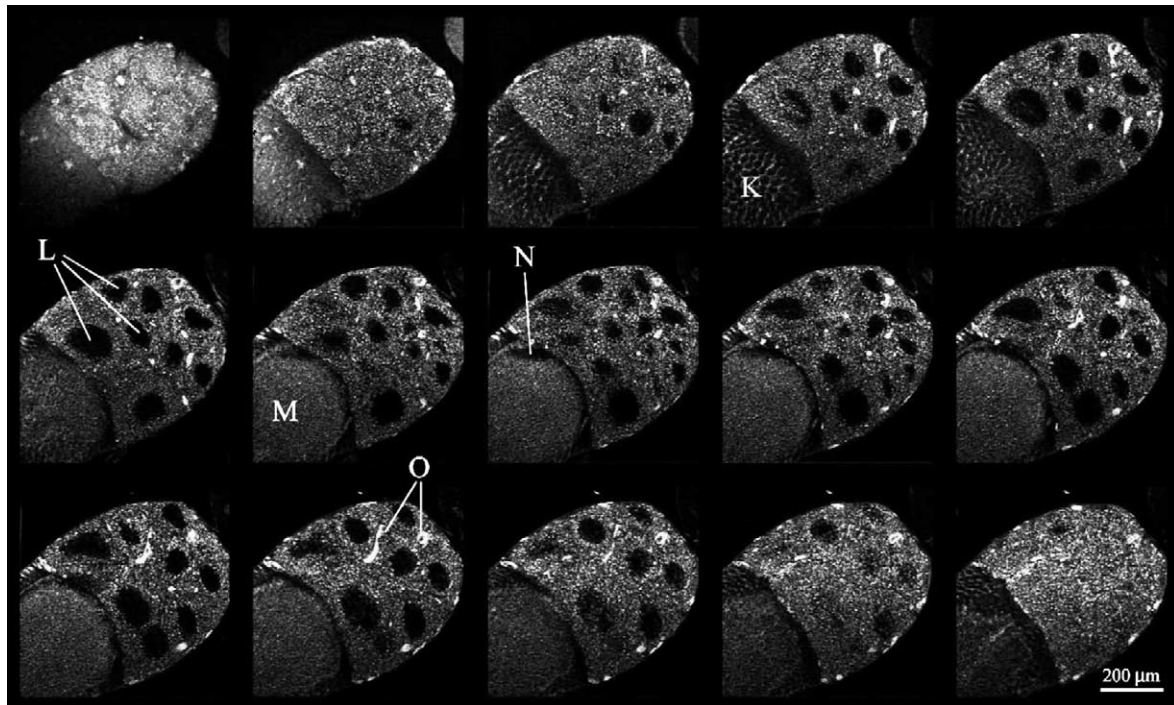Fig. 5. Fifteen $800 \times 800\,\mu m$ sections of a Drosophila egg chamber. The follicle cells (K), the nurse cells nuclei (L), the yolk (M), the oocyte (N), and several bright structures (O) are clearly noticed. Sections are separated by 10 μm.

sections of an albino *Xenopus laevis* (South African frog) embryo's head are presented in Fig. 3. The sections are ordered according to their relative location along the *z*-axis, where the upper-left section is the closest to the objective lens and the bottom-right is the more distant part of the embryo. A close look at the sections reveals many internal organs such as otic vesicle (A), notochord (B), foregut (C), brain ventricle (D), heart anlage (E), head mesenchyme (F), and branchial arches (G).

Analysis of experiments with bones at very early embryonic developmental stages is usually done using standard histological techniques, in which the bone is cut into thin slices and then imaged with a standard microscope. Three-dimensional imaging of bones is difficult, mainly because of the high scattering cross section of the bone matrix. In Fig. 4 we show depth-resolved imaging of 17-day-old mouse bones by THG. The bones are 1–2 mm long and about 0.2–0.4 mm wide. Imaging was performed using a $NA = 0.45$ objective. The relative locations of the four sections, both in a side view, and in a top view, are schematically shown in Fig. 4A. The lighter parts in the sections shown in Figs. 4B and C seem to be the mineralized bone matrix. The darker 'voids' are attributed to (hypertrophic) cartilage cells, surrounded by the mineralized matrix. The section in Fig. 4C is from the center of the bone where less mineral is seen. That might be the primitive marrow cavity, an area that used to be mineralized as well, but was excavated by mineral removing cells—the osteo-clasts. Sections from the distal part of the bone are shown in Figs. 4D and E.

On a smaller scale, inhomogenities in biological organisms originate from the division into cells. THG microscopy allows imaging of such samples without using staining or fluorescence labeling. Furthermore, the use of a clearing solution is not required, as sample thickness is sufficiently small. Shown in Fig. 5 are 15 optical sections of a part of a Drosophila egg chamber, comprised of 15 nurse cells and a single oocyte, taken with a 40×, $NA = 0.65$ objective. The sections are separated by 10 μm in the *z*-axis. The follicle cells (K), the nurse cells nuclei (L), the yolk (M), the oocyte (N) and bright structures which may be related to the ring canals (O) are clearly visible. The nurse cells nuclei appear very dark compared with the cells' cytoplasms, as observed in most THG imaging experiments of single cells. We relate the low THG inside the nuclei to the absence of organelles or inhomogeneities of sizes on a micron scale at this region.

On yet a smaller scale, inhomogeneity within single cells is due to the distribution of various cellular organelles which have different compositions. Detailed examples of images of single cells can be found in Yelin and Silberberg (1999) and in Yelin et al. (2002).

In all the samples described above, the imaging relied on spatial inhomogeneity of the samples. In samples where strong optical anisotropy is present, such as in biogenic crystals, it is possible to image the local optical anisotropy by THG.

As described in the introduction, samples with strong birefringence can generate phase-matched THG even from a bulk medium. In both calcite and aragonite, the most common biogenic crystals, this condition can be fulfilled when the angle between the propagation direction of the illuminating beam and the fast (*c*-axis) of the
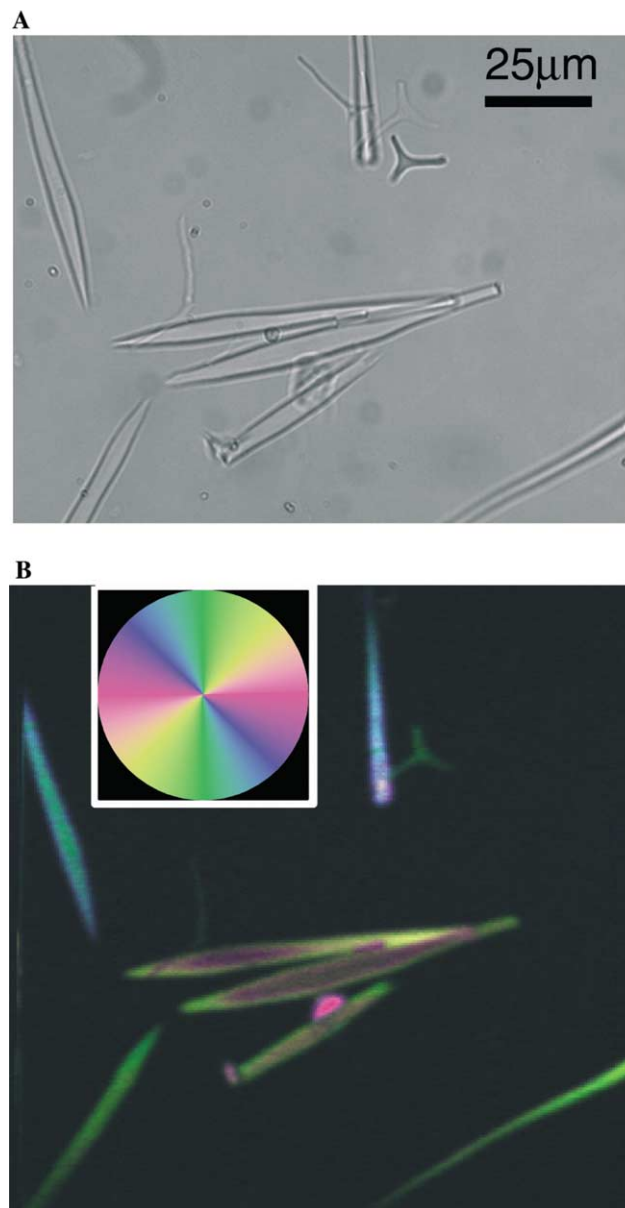

Fig. 6. A bright-field image (A) and a false-color polarization THG image (B) of sea-urchin larval spicules. In the THG image (B), linearly polarized THG is colored according to the color map given in the inset. For example, light polarized along the *x*-axis of the figure appears pink, while light polarized along the *y*-axis appears green. Circularly polarized signal appears gray or white, and elliptically polarized light has a fade color, determined by the direction of the major axis of the polarization ellipse.

crystal is greater than some critical angle. When the illuminating beam is focused entirely within a single crystal, the emitted THG is linearly polarized along the fast axis. When it is only partially focused within it, the THG polarization can be shifted from the fast axis by an amount which depends mostly on the focal depth of the objective. We illuminate the sample with circularly polarized light to eliminate the THG generated by isotropic media. The polarization configuration of the illumination beam and the third harmonic is schematically plotted in Fig. 2 for the case of calcite. When the beam propagates at a large angle with the extraordinary axis (Fig. 2A) the THG is polarized along the extraordinary axis and there is an observed change in the polarization of the illuminating beam. When the beam propagates along the extraordinary axis (Fig. 2B) no third-harmonic is generated and the input polarization remains unchanged. To determine the polarization state of the THG signal we perform four measurements, rotating the polarization analyzer at 45° between consecutive measurements. The four images are then processed by a computer to generate a false-color map showing the polarization orientation of the signal.

Images of fully crystalline fragments of sea-urchin larval spicules, from various growth stages, each comprised of a single calcite crystal are given in Fig. 6. A standard bright-field image is given in Fig. 6A, while a false-color THG polarization image is shown in Fig. 6B. The color map of the polarization state is given in the inset of Fig. 6B. According to this color map, a linearly polarized signal is colored according to the direction of the polarization. Thus, light polarized along the x-axis of the figure would appear pink, while light polarized along the y-axis would appear green. A circularly polarized signal appears gray or white, and elliptically polarized light (which can be decomposed into a circular component and a linear component) would have a fade color, determined by the direction of the major axis of the polarization ellipse. The brightness determines the signal intensity. The crystal c-axis of the larval spicules is aligned with the long dimension of body rods and is perpendicular to triradiates. Detailed examination of the image shows that in most spicules the color varies across the spicule. At the center of the spicule, where the specimen is sufficiently thick so that the illuminating beam is focused entirely within it, the color matches the orientation of the c-axis. At the edges, where the sample is thinner than the focal depth of the objective, the signal is polarized at up to 45° to the crystal c-axis, in a direction determined by the helicity of the illuminating beam. This relative polarization shift from the crystal c-axis direction where the sample is thin depends mainly on the focal depth of the objective lens. Triradiates do not fulfill the phase-matching condition. Indeed, a single triradiate can be seen to be much fainter (next to the blue spicule on the top right corner of the image).

The two THG techniques shown above can in fact be combined to map anisotropic regions within a mostly
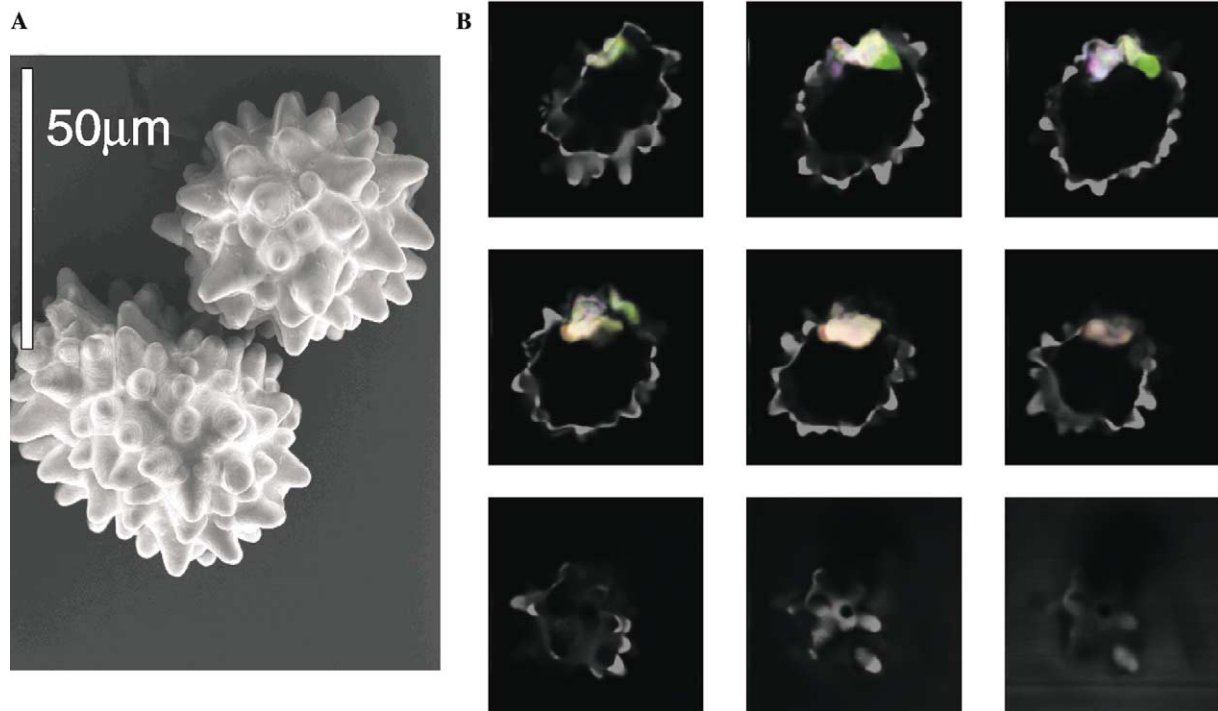

Fig. 7. (A) SEM image of two cystoliths. (B) Optical sections of a partially crystallized cystolith. A color polarization THG image is overlayed on a gray THG image obtained with linearly polarized light. The image area is $70 \times 70\,\mu m$ and sections are separated by $8\,\mu m$.

isotropic sample. Cystoliths are intracellular bodies composed of amorphous calcium carbonate and found in the leaves of certain trees. A SEM image of two such cystoliths is given in Fig. 7A. We induced partial crystallization in the cystolith by a short exposure to a humid environment. Two channels were combined in the optical cross sections of a partially crystallized cystolith given in Fig. 7B: the linearly polarized THG image is shown in gray, while the polarization THG measurements are overlayed on top of it in color. As can be seen, excluding the crystalline parts (bright colored areas appearing in some of the cross sections), the inside of the cystolith appears homogeneous. The outline of the cystolith appears as a strong signal from the index-matching oil–cystolith interface. The polarization THG images indicate that there are three crystalline regions with significantly different orientations, observed as blue, green, and yellow ones.

5. Conclusions

THG microscopy shares several inherent benefits with multiphoton fluorescence microscopy. It possesses intrinsic depth resolution due to the multiphoton nature of the process. Illumination is done with near-infrared light, which penetrates deeper into tissue on the one hand and induces less damage on the other. In practice, however, THG is more of a complimentary technique to multiphoton fluorescence microscopy. While fluorescence images provide information about specifically labelled sites within cells or organisms, THG provides structural information serving as a framework within which the fluorescence signals can be interpreted. Indeed, the combination of these two techniques has recently been reported (Chu et al., 2001; Chu et al., 2002; Yelin et al., 2002).

Since typically the THG signal vanishes in bulk media, this technique is both highly sensitive to structural inhomogeneity, and intrinsically background-free. Moreover, biological specimen are sufficiently inhomogeneous on all scales to provide rich structural information on virtually any sample.

The combination of polarization techniques and the THG technique is a promising tool to study biomineralization, due to the strong dependence of the THG signal on the optical anisotropy of the sample. In particular, strongly birefringent crystals such as calcite or aragonite produce a very strong, phase-matched signal whose polarization contains information on the crystal orientation.

Acknowledgments

References

Arnott, H.J., 1980. Carbonates in higher plants. In: Omori, M., Watabe, N. (Eds.), Mechanisms of Biomineralization in Animals and Plants. Tokai university press, Tokyo, pp. 211–218.

Barad, Y., Eisenberg, H., Horowitz, M., Silberberg, Y., 1997. Nonlinear scanning laser microscopy by third harmonic generation, Appl. Phys. Lett. 70, 922–924.

Boyd, R., 1992. Nonlinear Optics. Academic Press, New York.

Campagnola, P.J., Millard, A.C., Terasaki, M., Hoppe, P.E., Malone, C.J., Mohler, W.A., 2002. Three-dimensional high-resolution second-harmonic generation imaging of endogenous structural proteins in biological tissues. Biophys. J. 81, 493–508.

Canioni, L., Rivet, S., Sarger, L., Barille, R., Vacher, P., Voisin, P., 2001. Imaging of Ca^{+2} intracellular dynamics with a third-harmonic generation microscope. Opt. Lett. 26, 515.

Cheng, J.-X., Xie, X.S., 2002. Green's function formulation for third-harmonic generation microscopy. J. Opt. soc. Am. B 19, 1604–1610.

Chu, S.-W., Chen, I.-H., Liu, T.-M., Chen, P.C., Sun, K.C., 2001. Multimodal nonlinear spectral microscopy based on a femtosecond Cr:forsterite laser. Opt. Lett. 26, 1909–1911.

Chu, S.-W., Chen, I.-H., Liu, T.-M., Sun, K.C., Lee, S.-P., Lin, B.-L., Cheng, P.-C., Kuo, M.-X., Lin, D.-J., Liu, H.-L., 2002. Nonlinear bio-photonic crystal effects revealed with multimodal nonlinear microscopy. J. Microsc. 208, 190–200.

Cox, G., Kable, E., Jones, A., Fraser, I., Manconi, F., Gorrell, M.D., 2002. 3-Dimensional imaging of collagen using second-harmonic generation. J. Struct. Biol. 141, 53–62.

Denk, W., Strickler, J.H., Webb, W.W., 1990. Two-photon laser scanning fluorescence microscopy. Science 248, 73–76.

Gannaway, J., Sheppard, C.J.R., 1978. Second harmonic imaging in the scanning optical microscope. Opt. Quant. Electron. 10, 435–439.

Killian, C.E., Wilt, F.H., 1996. Characterization of the proteins comprising the integral matrix of Strongylocentrotus purpuratus embryonic spicules. J. Biol. Chem. 271, 9150–9159.

Maiti, S., Shear, J.B., Williams, R.M., Zipfel, W.R., Webb, W.W., 1997. Measuring serotonin distribution in live cells with three-photon excitation. Science 275, 530–532.

Muller, M., Squier, J., Wilson, K.R., Brakenhoff, G.J., 1998. 3D-microscopy of transparent objects using third-harmonic generation. J. Microsc. 191, 266–274.

Oron, D., Tal, E., Silberberg, Y., 2003. Depth resolved multiphoton polarization microscopy by third-harmonic generation, Opt. Lett., submitted.

Peleg, G., Lewis, A., Bouevitch, O., Loew, L., Parnas, D., Linial, M., 1996. Gigantic optical non-linearities from nanoparticle-enhanced molecular probes with potential for selectively imaging the structure and physiology of nanometric regions in cellular systems. Bioimaging 4, 215–224.

Penzkofer, A., Ossig, F., Qiu, P., 1988. Picosecond third-harmonic light generation in calcite. Appl. Phys. B 47, 71–81.

Shelton, J.W., Shen, Y.R., 1972. Study of phase-matched normal and umklapp third-harmonic-generation processes in cholesteric liquid crystals. Phys. Rev. A. 5, 1867–1882.

Yakovlev, V.V., Govorkov, S.V., 2001. Diagnostics of surface layer disordering using optical third harmonic generation of a circular polarized light. Appl. Phys. Lett. 79, 4136–4138.

Yelin, D., Silberberg, Y., 1999. Laser scanning third-harmonic-generation microscopy in biology. Opt. Express. 5, 169–175.

Yelin, D., Oron, D., Korkotian, E., Segal, M., Silberberg, Y., 2002. Third-harmonic microscopy with a titanium–sapphire laser. Appl. Phys. B 74, s97–s101.

Yelin, D., Silberberg, Y., Barad, Y., Patel, J.S., 1999a. Depth-resolved imaging of nematic liquid crystals by third harmonic microscopy. Appl. Phys. Lett. 74, 3107–3109.

Yelin, D., Silberberg, Y., Barad, Y., Patel, J.S., 1999b. Phase-matched third-harmonic generation in a nematic liquid crystal cell. Phys. Rev. Lett. 82, 3046–3049.

Zoumi, A., Yeh, A., Tromberg, B.J., 2002. Imaging cells and extracellular matrix in vivo by using second harmonic generation and two-photon excited fluorescence. Proc. Natl. Acad. Sci. 99, 11014–11019.

Zumbusch, A., Holtom, G.R., Xie, X.S., 1999. Three-dimensional vibrational imaging by coherent anti-Stokes Raman scattering. Phys. Rev. Lett. 82, 4142–4145.